Resonant Auger decay of Ar $2p_{3/2}^{-1}4s$ and $2p_{3/2}^{-1}4p$ states excited by electron impact

B. Paripás* and B. Palásthy
Department of Physics, University of Miskolc, H-3515 Miskolc-Egyetemváros, Hungary

M. Štuhec and M. Žitnik
Jožef Stefan Institute, P. O. Box 3000, SI-1001 Ljubljana, Slovenia

(Received 4 August 2010; published 22 September 2010)

Auger spectra of resonantly excited $2p_{3/2}^{-1}4s$ and $2p_{3/2}^{-1}4p$ states in argon were measured by $(e,2e)$ technique. The 99.2-eV scattered electrons were detected in coincidence with L_3–$M_{23}M_{23}$ Auger electrons, and the experiment was performed at 343.6- and 344.9-eV electron impact to tune the energy loss to the energy of the dipole-allowed and the dipole-forbidden excitations, respectively. The resonant Auger spectra are obtained upon subtraction of the overlapping signal due to the outer-shell ionization, which was recorded at 340-eV electron-impact energy. The most intense groups of Auger transitions from $2p_{3/2}^{-1}4s$ ($J=1,2$) and $2p_{3/2}^{-1}4p$ ($J=0,1,2,3$) states are identified by comparison with the results of the two-step model, based on distorted-wave Born approximation with exchange and multiconfiguration descriptions of the relaxed states. The $4s$ spectrum displays a substantially larger shake-up contribution than the one observed in photoexcitation experiments, which may be explained by the interference of the resonant decay path with the direct ionization excitation of the Ar $3p$ subshell. The majority of the observed $4p$ signal is assigned to the monopole and quadrupole excitations of the ground state.

DOI: 10.1103/PhysRevA.82.032508 PACS number(s): 32.30.−r, 34.80.Dp, 34.80.Pa

I. INTRODUCTION

Atomic resonances are most often studied by a photon probe because then the energy transfer to the atom is well defined—it equals energy of a photon, which is absorbed. By a precise energy tuning of the monochromatic photon beam, one can selectively excite specific types of resonances and investigate their decay paths. In the case of an electron impact, however, an exact amount of energy and angular momentum transfer in a particular scattering event are not predictable. This fact prevents resonant studies by simple experiments where only an electron-impact energy is selected. At least the scattered electron energy has to be measured too, and to investigate the decay of the selectively excited state further, decay products have to be measured in coincidence with electrons submitted to the resonant energy loss. The study of resonant Auger decay at a given electron-impact energy E_0 therefore requires an $(e,2e)$ experiment, in which the energy-selected scattered electron is detected in coincidence with the ejected Auger electron over the whole spectral range of the latter.

In the course of inelastic electron scattering on argon, one electron from the $2p$ subshell may be transferred to a vacant nl Rydberg state,

$$e_1^-(E_0) + \mathrm{Ar} \rightarrow e_1^-(E_a) + \mathrm{Ar}^*[2p_{3/2,1/2}]nl(J), \qquad (1)$$

when the energy loss $E_0 - E_a$ matches the excitation energy E_α of the selected resonance. These excited states decay most probably by L–$M_{23}M_{23}$ Auger process: While one $3p$ electron fills the $2p$ vacancy, another $3p$ electron, the resonant Auger electron, is ejected into continuum. Due to the presence of an outer electron, the resonant Auger spectra are shifted to higher energies and display more complex structures than the ordinary L–$M_{23}M_{23}$ spectrum, which proceeds from the pure $2p$ vacancy [1,2]. As a consequence of energy conservation, the resonant Auger lines follow the selected electron energy loss, which is a well-known characteristic from photoexcitation experiments [3,4]. The final $\mathrm{Ar}^+[3p^2]$ states are strongly correlated and require a rich basis of single configuration states for a proper description [5,6]. The Rydberg orbitals of the intermediate and of the final states differ considerably, which triggers the additional dynamics—during the Auger decay, the Rydberg electron either remains in the occupied nl orbital (spectator), or jumps with a non-negligible probability into the other $n'l$ orbital (participator decay).

The energy positions of the lowest excited atomic states, built on the $2p_{3/2}$ and $2p_{1/2}$ core holes of argon [7], are shown in Fig. 1 together with the horizontal bars indicating the full width at half maximum (FWHM) energy resolution of our experimental apparatus. The energy separation of the adjacent excited states is smaller than FWHM, except for the $[2p_{3/2}]4s$ and $[2p_{3/2}]4p$ states, which are separated enough to be effectively isolated by our $(e,2e)$ spectrometer.

The most probable resonant decay paths involving two (groups of) excited states selected for this study are written as (using simplified single configuration description of final states)

$$e_1^-(E_0) + \mathrm{Ar} \rightarrow e_1^-(E_a) + \mathrm{Ar}^*[2p_{3/2}]4s(J) \rightarrow e_1^-(E_a) + \mathrm{Ar}^{+*}[3p^2(^1S,^3P,^1D)]4(\mathrm{or}\ 5)s + e_2^-(E_b), \qquad (2)$$

and

$$e_1^-(E_0) + \mathrm{Ar} \rightarrow e_1^-(E_a) + \mathrm{Ar}^*[2p_{3/2}]4p(J) \rightarrow e_1^-(E_a) + \mathrm{Ar}^{+*}[3p^2(^1S,^3P,^1D)]4(\mathrm{or}\ 5)p + e_2^-(E_b). \qquad (3)$$

*fizpari@uni-miskolc.hu

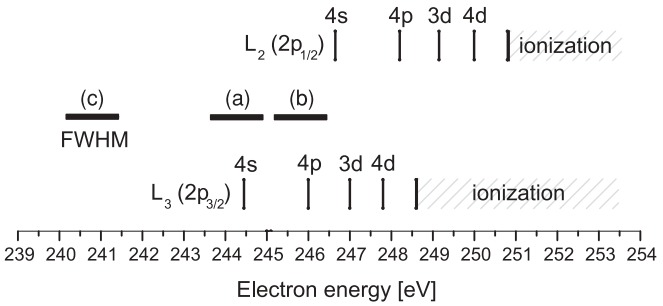

FIG. 1. Excitation energies E_α of Ar[$2p$]nl states and the energy-transfer windows selected by our experiment: (a) 244.4 ± 0.6 eV, (b) 245.7 ± 0.6 eV, (c) 240.8 ± 0.6 eV.

The question arises whether all the detected electron pairs, which populate final ionic states (2) and (3), originate from resonant excitation. The answer is definitely not because the same final states can also be formed directly by $3p$ ionization, which is accompanied by an excitation of another $3p$ electron:

$$e_1^-(E_0) + \mathrm{Ar} \rightarrow \mathrm{Ar}^{+*}[3p^2(^1S,^3P,^1D)]nl + e_1^-(E_a) + e_2^-(E_b). \quad (4)$$

Different from photoexcitation [6,8], the probability of the outer-shell satellite ionization by an electron impact is relatively high even far from its threshold. As shown subsequently, it is in fact higher than the probability of the $2p$ resonant Auger process and has to be taken into account. In contrast to the two-step process, the electrons in the final state (4) share their energy in a continuous manner. The corresponding coincidence peaks recorded by two electron spectrometers (one fixed in energy and the other energy scanning) therefore move in energy when the electron-impact energy is changed. However, the electron-impact energy dependence of the outer-shell satellite ionization is relatively weak, and this is particularly true for our experimental conditions, as the electron-impact energy is larger than the binding energy of the final ionic state by an order of magnitude. The spectrum of a nonresonant process Eq. (4) measured in window (c) (Fig. 1) is expected to have practically the same shape as the spectrum of the same process measured in window (a) or (b) except that the spectra are shifted in energy by an amount that exactly corresponds to the shift of the electron-impact energy. The only difference in the pair of measured spectra therefore comes from the contribution of the resonant process. In other words, the measured spectrum in window (c) represents the direct ionization background underlying the resonant Auger spectra measured in windows (a) and (b). The signal due to direct ionization also is present in a noncoincidence Auger spectrum, but there it appears as a structureless background and can easily be subtracted.

The coincidence electron yields from the direct and resonance processes are, in principle, not additive quantities because quantum-mechanical interference takes place between different paths leading to the same final state. Due to comparable amplitudes, this interference could have a considerable effect on the spectrum in our case, and the two processes might not be separable. On the other hand, we speculate that relatively large accepted solid angle and broad energy acceptance of our experimental setup may average out these bound-continuum interference effects so that the difference of on-the-resonance and off-the-resonance signals can be interpreted as a pure resonant Auger spectrum.

In the past, a few hints about the resonant component of the L–MM Auger process were obtained by *noncoincidence* experiments performed at several electron-impact energies above the Ar L threshold [9,10]. These measurements aimed to separate very weak resonant signals from the signal of the diagram Auger lines. The effort was supported by an elaborate fitting procedure and pointed to several spectral features that could originate from the decay of [$2p_{3/2}$]$4s$,$4p$ states. In contrast to the number of theoretical and experimental photoexcitation studies, dealing with the characterization of highly resolved Auger spectra of $J=1$ resonances in argon (Refs. [11,12] and references therein), the studies of the corresponding processes induced by an electron impact are not yet reported, except for our recent demonstration of the $(e,2e)$ approach in the region of the $2p$ threshold [13]. However, the electron-electron coincidence technique was extensively used to study decay of the lowest autoionizing resonances in helium [14], and for heavier atoms, the $(e,2e)$ work related to autoionizing resonances of Cd is reported [15]. The resonant Auger decay of core-hole molecular states was studied by an electron impact, aiming, for example, to separate the processes mediated by the lowest triplet-singlet pair of core-hole excited states in CO and N_2 [16,17]. Regarding the inner-shell excited atomic states, we are aware only of the work of Avaldi *et al.* [18] who related a part of the $(e,2e)$ signal acquired close to the xenon $4d$ threshold to the resonant Auger decay of [$4d$]nl states.

In the following, we give a detailed report about coincidence measurements of the lowest two groups of [$2p_{3/2}$]$nl(J)$ resonances in argon, which were separately excited by the energy-selected electron-beam impact. These resonant processes occur at about 245-eV energy loss and are observed at relatively large scattering angles. Thus, the corresponding $(e,2e)$ cross sections are very low, as evidenced by the previous noncoincidence measurement estimating about 1% contribution of the resonant process relative to the L_3–$M_{23}M_{23}$ diagram Auger decay at similar electron-impact energy [9]. Moreover, the excitation of the [$2p_{3/2}$]$4p(J)$ group of states by photons is forbidden, and there are yet no corresponding resonant Auger spectra reported in the literature. To assign different spectral features, the experimental results are compared to the results of the two-step model, which treats the inelastic electron scattering and the Auger decay as two independent steps of the resonant process.

II. EXPERIMENT

Our coincidence spectrometer was described previously [19], and only a few basic parameters are given here: a single pass cylindrical mirror analyzer (CMA) spectrometer (A) and a double-pass CMA spectrometer (B) are mounted on the same axis, which is perpendicular to the electron projectile beam (Fig. 2). Target is formed by an effusive gas source placed in between the spectrometer's entrances. Large acceptance solid angles of CMA ($\approx$0.18 sr), essential to accumulate statistically significant data in reasonable time, are provided by 5°-wide entrance cones. The entrance angle

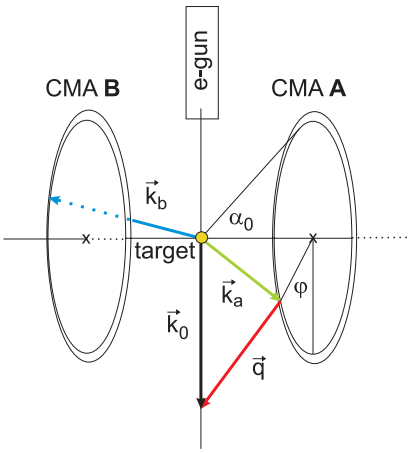

FIG. 2. (Color online) Schematic of $(e,2e)$ experimental setup employed for spectroscopy of resonant Auger process.

with respect to the CMA axis is close to $\alpha_0 = 43.5^\circ$. The coincidence electron spectra were measured by changing the transmission energy E_B of the spectrometer B in the energy region of Auger electrons, while the scattered electrons were detected by the spectrometer A whose transmission energy E_A was kept fixed. In the present measurements, the energy of the scattered electrons was 99.2 ($\pm$0.5) eV, thus the energy-transfer windows in Fig. 1 were realized at (a) 343.6-, (b) 344.9-, and (c) 340.0-eV electron-impact energies. We remark that window (b) is set slightly asymmetric with respect to the $[2p_{3/2}]4p$ resonant energy in order to avoid $[2p_{1/2}]4s$ contribution to the spectrum.

As mentioned, the resonant Auger spectrum is obtained by subtraction of the direct ionizing background from the $(e,2e)$ spectrum taken under resonance conditions [Fig. 3(a)]. The most intense satellite peaks were identified before [20] on the basis of high-resolution photoelectron data [21]. Prior to subtraction, the coincidence yields were normalized to the yield of the 99.2-eV electrons acquired by spectrometer A, while the direct ionizing background was shifted by the difference of electron-impact energies (i.e., by 3.6 and 4.9 eV, respectively, to align the $[3s]$ coincidence peak in both spectra [Fig. 3(a)]). The final result for both groups of resonances is shown in Figs. 3(b) and 3(c). Although the net coincidence spectra contain hardly more than 10^4 counts, their collection required about 100 days of acquisition time with the total number of counts on the order of 10^{10}. The contribution of false coincidences was about 35% and was removed from the spectra.

The weak lines previously found by noncoincidence measurements [9] are the dominant spectral features in the present spectra (denoted by arrows). The signal leading to $[3p^2\ ^3P]nl$ final states is expected to be found at about 1.6 eV above the $[3p^2\ ^1D]nl$ states. These ^3P lines can actually be discerned at 211.6 eV [Fig. 3(b)] and at 210.2 eV [Fig. 3(c)], respectively. In resonant Auger process, the shake process is often activated. In our case, the $4s \rightarrow 5s$ shake-up shifts down the Auger lines by 6.6 eV, and the corresponding lines are expected to be situated at 203.4 eV ($[3p^2\ ^1D]5s$) and at 205 eV ($[3p^2\ ^3P]5s$). Indeed, some signal is detected in the vicinity of the previous energies in Fig. 3(b). We note that by outer-shell

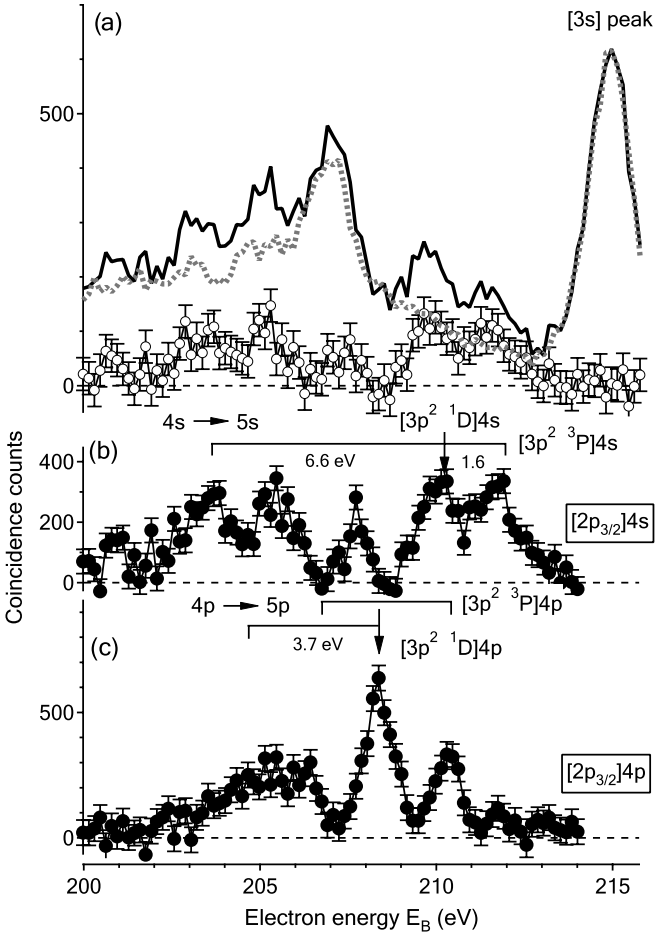

FIG. 3. (a) Off-the-resonance coincidence signal (gray-dotted line, $E_0 = 340.0$ eV, $E_A = 99.2$ eV) was shifted in energy and scaled to the coincidence signal taken under $[2p_{3/2}]4s$ resonant conditions (black line, $E_0 = 343.6$ eV, $E_A = 99.2$ eV) to match the $[3s]$ ionization peak. The difference of the two signals (empty circles) is assigned to the resonant Auger decay of $[2p_{3/2}]4s$. (b) The final resonant Auger spectrum of $[2p_{3/2}]4s$. (c) The final resonant Auger spectrum of $[2p_{3/2}]4p$. Arrows denote peaks observed previously by the noncoincidence experiment [9], and a tentative assignment is given (see text).

photoionization, an energy difference of 5.8 eV was found between the corresponding $[3p^2]4s$ and $[3p^2]5s$ states [22], which is smaller than the shift we found.

Although the excitation energy of the Ar$[2p_{3/2}]4p(J)$ group of states is long known from high-resolution electron energy-loss measurement (EELS) [7], no data related to decay of this dipole-forbidden state are available. The relative probability of the $4p \rightarrow 5p$ shake-up process and the corresponding energy shift are unknown, but the latter can be estimated by means of the outer-shell photoionization data. The energy difference between the corresponding $[3p^2]4p$ and $[3p^2]5p$ terms is 3.7 eV [22]. Since the lines corresponding to $[3p^2\ ^1D]4p$ and $[3p^2\ ^3P]4p$ peaks are found at 208.6 and 210.2 eV, respectively, the corresponding shake-up lines are expected at 204.9 and 206.5 eV. In Fig. 3(c), the lines are well discernible in the vicinity of predicted energies. Relative intensity of these participator lines with respect to spectator

lines suggests a considerable probability for the $4p \rightarrow 5p$ shake-up process.

III. THEORY AND COMPARISON OF RESULTS

To interpret the measured resonant Auger spectra, a two-step model is employed, which treats the process as a sequence of two independent steps (excitation emission). In addition, the model neglects target alignment due to electron scattering and assumes isotropic Auger electron emission. The triple differential cross section, which involves an intermediate state α (with a natural linewidth $\Gamma_\alpha \approx 120$ meV, [23]) and a final state β (with a negligible natural linewidth) is then approximated by

$$\frac{d^3\sigma_{\alpha,\beta}}{d\Omega_a\, d\Omega_b\, dE_a} = \frac{d^2\sigma_\alpha}{d\Omega_a\, dE_a}\frac{\sigma^A_{\alpha\beta}}{4\pi}\delta(E_0 - E_a - E_b - E_\beta), \tag{5}$$

where $\sigma^A_{\alpha\beta}$ is the total cross section for $\alpha \rightarrow \beta$ Auger transition and

$$\frac{d^2\sigma_\alpha}{d\Omega_a\, dE_a} = \eta_\alpha(\Omega_a)\frac{\Gamma_\alpha/(2\pi)}{(E_\alpha - E_0 + E_a)^2 + \Gamma_\alpha^2/4} \tag{6}$$

is the doubly differential inelastic electron-scattering cross section (DDCS) for excitation of resonance α at electron-impact energy E_0. The measured coincidence yield $C_{\alpha\beta}$ at nominal transmission energies E_A and E_B is obtained upon integration of Eq. (5) over the accepted solid angle of spectrometer A and convolution by energy-dependent (Gaussian) spectrometer transmission functions,

$$C_{\alpha\beta}(E_A, E_B) \propto \sigma^A_{\alpha\beta} N^A_\alpha \exp\left[-\frac{(E_A - E_\alpha - E_0)^2}{2\sigma_A^2}\right] \times \exp\left[-\frac{(E_B - E_\alpha - E_\beta)^2}{2\sigma_B^2}\right]. \tag{7}$$

Earlier,

$$N^A_\alpha(E_A) = \int_{\Delta\Omega_A} d\Omega_A\, \eta_\alpha(\Omega_a) \tag{8}$$

is the effective excitation strength of resonance α that weakly depends on the energy of the incoming and scattered electrons. We have assumed that DDCS displays a simple resonant (Lorentzian) behavior within the fixed energy transmission window of spectrometer A and that the natural linewidth Γ_α is much larger than FWHM ($\approx 2.35\sigma_A$).

A. Excitation strengths

The first step toward the model spectrum is to calculate relative excitation strengths N_α of low-lying resonances. These theoretical values can be compared to N_α values, extracted from the fit of the electron energy-loss spectrum Y, recorded by spectrometer B in a separate electron energy-loss measurement at $E_0 = 350$ eV [13],

$$Y(E_B) = \sum_\alpha \exp\left[-\frac{(E_B - E_\alpha - E_0)^2}{2\sigma_B^2}\right] N^B_\alpha. \tag{9}$$

Different from the electron-impact excitation of outer shells [24], the measurements of generalized oscillator strengths (GOSs) for $2p$ electron-impact excitation in Ar are scarce and incomplete. Apart from Shaw *et al.* [23] who reported the evolution of high-resolution EELS in the forward direction for three different values of the momentum transfer $q = |\mathbf{k}_0 - \mathbf{k}_a|$ (0.90, 1.74, and 2.30 a.u.), the only other experimental work was performed at $E_0 = 2.5$ keV [25]. GOS for the $2p_{3/2} \rightarrow 4s$ transition was measured for different scattering angles going from 1.5° to 8° ($q = 0.6 - 2.2$ a.u.), and fine agreement was found with GOSs calculated in the frame of the first Born approximation [26]. These calculations also predicted zero GOS value, related to the nodal structure of the radial part of the atomic orbitals of the ground and excited states, similar to the Cooper minimum known from photoelectron [27] and proton-induced x-ray emission [28]. While none of the previous experiments reached $q = 3.51$ a.u. at which the minimum occurs, our experiment at $E_0 = 350$ eV [13] is characterized by even larger values of momentum transfer $q \approx 4 - 9$ a.u.

Besides the dipole excitations of $|g\rangle$, the ground state of argon, other multipole excitations may be induced by electron scattering. In general, the share of the forbidden transitions increases with the electron momentum transfer q. The total angular momentum $J = 1,2$ is possible for Ar$[2p_{3/2}]4s$ resonance, but dipole-allowed $J = 1$ is expected to be the dominant excitation channel at high electron-impact energy and/or small scattering angles. The situation is less clear for $[2p_{3/2}]4p$ resonance, since the transitions from the ground state to $[2p_{3/2}]4p$ with possible values of $J = 0,1,1,2,2,3$ are all forbidden to a certain extent. Energy splitting of different J terms for the latter configuration is calculated to be 78 meV, which is smaller than Γ_α, and different contributions are not resolved even by the high-resolution EELS [7]. On the basis of measured intensity ratio of $[2p_{3/2}]4p$ versus $[2p_{3/2}]4s$ excitation as a function of q, Shaw *et al.* [23] suggested that $J = 0$ and $J = 2$ levels are mostly excited through the quadrupole part of the Coulomb interaction. Indeed, the plane-wave Born approximation (PWBA) with a single configuration description of the ground and excited $[2p]4p$ states allows only a transfer of 0 or 2 units of orbital angular momentum due to the electron scattering.

To predict experimental yields, we have calculated GOSs for several low-lying $2p \rightarrow nl$ transitions in PWBA:

$$f_\alpha = \frac{2E_\alpha}{q^2}\left|\langle\alpha|\sum_j e^{-i\mathbf{q}\mathbf{r}_j}|g\rangle\right|^2_{\text{av}}. \tag{10}$$

The procedure implies averaging over the initial and summing over the final projections of angular momenta. When small differences between the excitation energies of different states are neglected, a single configuration description of the ground and of excited states with orthogonal orbitals leads to the following expressions:

$$\frac{f_{ns}}{f_{np}} = \frac{R^2_{ns}(1)}{R^2_{np}(0) + 2R^2_{np}(2)}, \quad \frac{f_{ns}}{f_{nd}} = \frac{R^2_{ns}(1)}{2R^2_{nd}(1) + 3R^2_{nd}(3)}. \tag{11}$$

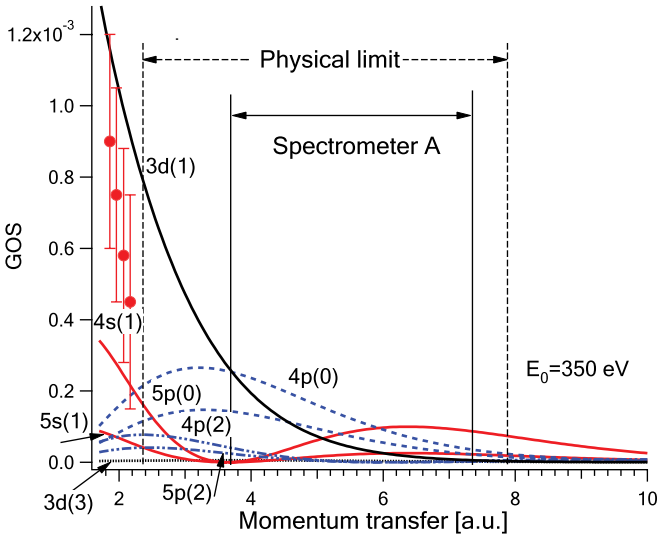

FIG. 4. (Color online) GOSs for $2p \rightarrow 4-5s$ (red), $2p \rightarrow 4-5p$ (blue), and $2p \rightarrow 3d$ (black) transitions in Ar as a function of electron momentum transfer, calculated by PWBA in the length form with a single configuration description of atomic states. For comparison, the only available experimental data points are shown for the $2p_{3/2} \rightarrow 4s$ transition at $E_0 = 2.5$ keV [25]. The range of the momentum transfer observed by spectrometer A at an electron-impact energy of 350 eV is denoted, as well as the physical limit $q_{\min} = k_0 - k_a$. The $[2p]nl$ excited state and the angular momentum transfer L are shortly denoted by $nl(L)$.

In radial integrals

$$R_{nl}(L) = \int_0^\infty P_{2p}(r) j_L(qr) P_{nl}(r)\, dr,$$

j_L denotes the spherical Bessel function of Lth order and P_{nl} is a radial orbital of electron in an nl subshell. The use of this simple approximation is supported by the configuration interaction calculations that do not show any significant mixing for singly excited states. GOSs for several transitions calculated with Hartree-Fock orbitals are presented in Fig. 4 for different values of the momentum transfer. While the velocity form approximately reproduces the $4s_{3/2}$:$3d_{3/2}$ line intensity ratio in the optical limit [29], the length form strongly underestimates this ratio, and GOS for $2p \rightarrow 4s_{3/2}$ transition is below the value of 7.84×10^{-3}, calculated by the configuration interaction PWBA approach in the optical limit [26]. The Hartree-Fock $4s$ orbital therefore more accurately describes the wave function close to the nucleus than in the outer atomic region. At large q, this deficiency becomes less important; due to the fast oscillations of $j_L(qr)$, the radial interval, which contributes the most to the integral moves inward and makes the length form more reliable.

DDCS is related to the differential GOS by the Bethe-Born formula [30]. However, the magnitude of momentum transfer strongly depends on the CMA polar angle φ (Fig. 2),

$$q(\varphi) = \sqrt{k_0^2 + k_a^2 - 2k_0 k_a \sin\alpha_0 \cos\varphi}, \qquad (12)$$

so that finally [31],

$$N_\alpha = \frac{2k_a}{k_0 E_\alpha} \int_0^{\Delta\varphi} \frac{f_\alpha(q, E_\alpha)}{q^2}\, d\varphi, \qquad (13)$$

where $\Delta\varphi$ is the CMA polar acceptance angle (Fig. 2).

According to PWBA, the np lines are mostly excited by the zero transfer of (orbital) angular momentum ($L = 0$) and less likely by the transfer of two units of angular momenta ($L = 2$), showing that the monopole transition is by far the most dominant mode of $[2p]4p$ excitation at 350 eV. Similarly, for nd states, the transfer of three units of angular momentum $L = 3$ is less probable than the $L = 1$ option, at least for $q < 10$ a.u. (Fig. 4).

In the simple PWBA model, the transfer of one unit of angular momentum ($L = 1$) is the only option for ns excitation, since the exchange interaction with the projectile is neglected. According to Shaw *et al.* [23], this is a reasonable assumption until $E_0 > 350$ eV, but our experimental setup detects scattered electrons at much larger angles where the importance of the exchange interaction is expected to increase. As shown by the photoabsorption data [29], the spin-orbit effect is mainly manifested by $2p_{3/2}$–$2p_{1/2}$ energy splitting, and relative intensities of corresponding lines obey the statistical ratio of 2:1 well. However, to describe the excitation strengths of overlapping resonances with different total angular momentum J more accurately (that populate different final states by the Auger decay), we have employed distorted-wave Born approximation (DWBA) with exchange [32]. This approximation also takes into account the projectile scattering by atomic potential, another effect that may considerably affect the DDCS at 350-eV electron-impact energy.

For this purpose, the excited states are described by jjJ-coupled single configurations, which are then converted to a jKJ scheme to represent the physical resonances. We proceed to calculate the scattering amplitude T for the process where the projectile electron has spin projection m_{s0} and m_{a0} before and after the collision, respectively, and the Ar atom is excited from the $J = 0$ ground state to the state with orbital angular momentum L_i (and projection M_{Li}) and the total spin S_i (and projection M_{Si}):

$$\begin{aligned} &T_{0m_{s0}}^{L_i S_i m_{sa}}(l_i, l_f, M_{Li}, M_{Si}) \\ &= \sum_{m_i m_f m_{si} m_{sf}} \Bigg[\langle l_f m_f l_i m_i | L_i M_{Li} \rangle \left\langle \frac{1}{2} m_{sf} \frac{1}{2} - m_{si} \middle| S_i M_{Si} \right\rangle \\ &\quad \times \langle l_i m_i l_i - m_i | 00 \rangle \left\langle \frac{1}{2} m_{si} \frac{1}{2} - m_{si} \middle| 00 \right\rangle \\ &\quad \times \left\langle \chi_{\mathbf{k}_a}^- \{ \alpha_{l_i m_i (1/2) m_{si}}^{l_f m_f (1/2) m_{sf}} \} \middle| \sum_n \frac{1}{r_{0n}} \middle| \chi_{\mathbf{k}_0}^+ \{\alpha\} \right\rangle \Bigg]. \end{aligned} \qquad (14)$$

Curly brackets denote Slater determinants, and the corresponding lower index row denotes a single electron orbital replaced by the excited electron orbital after the scattering in the upper index row. To obtain the cross section, the preceding amplitudes are coupled to represent atomic states with the

specific total atomic angular momenta J_α,

$$
\begin{aligned}
&T_{0m_{s0}}^{J_\alpha M_\alpha m_{sa}}(l_i,l_f,L_i,S_i;\theta_a)\\
&\quad=\sum_{M_{Li}M_{Si}}\Bigg(\langle L_iM_{Li}S_iM_{Si}|J_\alpha M_\alpha\rangle\\
&\qquad\times\sum_{m_im_f}\Bigg\{\langle l_fm_fl_i-m_i|L_iM_{Li}\rangle\langle l_im_il_i-m_i|00\rangle\\
&\qquad\times\Bigg[A_{l_im_i}^{l_fm_f}(\theta_a)\delta_{m_{s0}m_{a0}}\sum_{m_s}\Bigg(\left\langle\frac{1}{2}m_s\frac{1}{2}-m_s\middle|S_iM_{Si}\right\rangle\\
&\qquad\times\left\langle\frac{1}{2}m_s\frac{1}{2}-m_s\middle|00\right\rangle\Bigg)-B_{l_im_i}^{l_fm_f}(\theta_a)\\
&\qquad\times\left\langle\frac{1}{2}m_{s0}\frac{1}{2}-m_{sa}\middle|S_iM_{Si}\right\rangle\left\langle\frac{1}{2}m_{sa}\frac{1}{2}-m_{sa}\middle|00\right\rangle\Bigg]\Bigg\}\Bigg).
\end{aligned}
\tag{15}
$$

The cross section for the excitation of state α is written as

$$
\frac{d^2\sigma_\alpha}{d\Omega_a\,dE_a}=(2\pi)^4\frac{k_a}{k_0}\frac{\sigma_{l_ij_il_fj_f}^{J_\alpha}(\Omega_a)\Gamma_\alpha/(2\pi)}{(E_\alpha-E_0+E_a)^2+\Gamma_\alpha^2/4},
\tag{16}
$$

where the single electron continuum wave functions are normalized to $\langle\chi_{\mathbf{k}}^-|\chi_{\mathbf{k}'}^+\rangle=\delta(\mathbf{k}-\mathbf{k}')$. Finally,

$$
\begin{aligned}
\sigma_{l_ij_il_fj_f}^{J_\alpha}(\Omega_a)=\frac{1}{2}\sum_{m_{s0}m_{a0}M_\alpha}\Bigg|\sum_{L_i,S_i}\sqrt{[j_i,j_f,L_i,S_i]}\\
\times\begin{Bmatrix}\frac{1}{2}&\frac{1}{2}&S_i\\ l_i&l_f&L_i\\ j_i&j_f&J_\alpha\end{Bmatrix}T_{0m_{s0}}^{J_\alpha M_\alpha m_{sa}}(l_i,l_f,L_i,S_i;\theta_a)\Bigg|^2,
\end{aligned}
\tag{17}
$$

where j_i and j_f are the total angular momentum of the active atomic electron prior and after the excitation, respectively, and θ_a is the scattering angle of the projectile. The results for different transitions $(l_i,j_i)\rightarrow(l_f,j_f)$ leading to excited atomic states with total angular momentum J_α can be expressed by the direct two-electron matrix elements $A_{l_im_i}^{l_fm_f}$:

$$
\begin{aligned}
&\left\langle\chi_{\mathbf{k}_a}^-(\mathbf{r}_0)\phi_{n_fl_fm_f}(\mathbf{r}_1)\middle|\frac{1}{r_{12}}\middle|\chi_{\mathbf{k}_0}^+(\mathbf{r}_0)\phi_{n_il_im_i}(\mathbf{r}_1)\right\rangle\\
&\quad=\frac{2}{\pi}\sqrt{[l_i,l_f]}\sum_{l_al_0K}\Bigg\{(-1)^{l_a+m_f}i^{l_a+l_0}\sqrt{[l_a,l_0]}e^{i(\sigma_{l_0}+\sigma_{l_a})}\\
&\qquad\times\begin{pmatrix}l_f&K&l_i\\-m_f&m_f-m_i&m_i\end{pmatrix}\\
&\qquad\times\begin{pmatrix}l_a&K&l_0\\-m_f+m_i&m_f-m_i&0\end{pmatrix}\\
&\qquad\times\begin{pmatrix}l_f&K&l_i\\0&0&0\end{pmatrix}\begin{pmatrix}l_a&K&l_0\\0&0&0\end{pmatrix}G_{l_al_0}^K(n_fl_f,n_il_i)\\
&\qquad\times Y_{l_a,-m_f+m_i}(\hat{k}_a)Y_{l_0,0}(\hat{k}_0)\Bigg\},
\end{aligned}
\tag{18}
$$

and by the two-electron exchange matrix elements $B_{l_im_i}^{l_fm_f}$:

$$
\begin{aligned}
&\left\langle\chi_{\mathbf{k}_a}^-(\mathbf{r}_1)\phi_{n_fl_fm_f}(\mathbf{r}_0)\middle|\frac{1}{r_{12}}\middle|\chi_{\mathbf{k}_0}^+(\mathbf{r}_0)\phi_{n_il_im_i}(\mathbf{r}_1)\right\rangle\\
&\quad=\frac{2}{\pi}\sqrt{[l_i,l_f]}\sum_{l_al_0K}\Bigg[(-1)^{l_a+m_i!-m_f}i^{l_a+l_0}\sqrt{[l_a,l_0]}e^{i(\sigma_{l_0}+\sigma_{l_a})}\\
&\qquad\times\begin{pmatrix}l_f&K&l\\0&0&0\end{pmatrix}\begin{pmatrix}l_a&K&l_i\\0&0&0\end{pmatrix}\begin{pmatrix}l_f&K&l_0\\m_f&-m_f&0\end{pmatrix}\\
&\qquad\times\begin{pmatrix}l_a&K&l_i\\m_f-m_i&-m_f&m_i\end{pmatrix}\\
&\qquad\times D_{l_al_0}^K(n_fl_f,n_il_i)Y_{l_a,-m_f+m_i}(\hat{k}_a)Y_{l_0,0}(\hat{k}_0)\Bigg].
\end{aligned}
\tag{19}
$$

The direct and exchange radial Slater integrals are denoted by G and D, respectively, and they were calculated for a given multipole order K, partial waves l_0 and l_a of the incoming and outgoing electrons with energies $k_0^2/2$ and $k_a^2/2$, respectively, and for the selected inner hole n_il_i and final excited electron orbital n_fl_f,

$$
\begin{aligned}
G&=\int\int dr_1\,dr_2\,P_{n_fl_f}(r_1)P_{E_al_a}(r_2)\frac{r_<^{K+1}}{r_>^K}P_{n_il_i}(r_1)P_{E_0l_0}(r_2),\\
D&=\int\int dr_1\,dr_2\,P_{n_fl_f}(r_2)P_{E_al_a}(r_1)\frac{r_<^{K+1}}{r_>^K}P_{n_il_i}(r_1)P_{E_0l_0}(r_2).
\end{aligned}
\tag{20}
$$

The continuum radial partial waves P_{El} were calculated in the ground-state potential for $l_0,l_a\leqslant 40$. The corresponding phase differences with respect to the plane-wave radial waves $j_l(kr)$ are denoted by σ_{l_0} and σ_{l_a}. For the smallest angular momenta l, they differ considerably from zero indicating a strong effect of electron scattering on the atomic potential.

The cross sections expressed in terms of the direct and exchange amplitudes are given in the Appendix (Table I). It is evident that the forbidden values of angular momenta ($J=0,2$ for $[2p]ns$ and $J=1,3$ for $[2p]np$ states) can be transferred only through the projectile exchange with the target electron. In Fig. 5, we present the calculated double differential cross section for excitation of Ar $[2p]4s$ ($J=0,1,1,2$) states by 350-eV electron impact. Although the exchange amplitude is negligible for the forward electron scattering, it becomes comparable to the direct amplitude at scattering angles observed by our spectrometers. The comparison shows that DWBA shifts scattering intensity toward larger scattering angles with respect to PWBA. A discrete part of EELS spectrum (9) is given by the doubly differential cross section summed over the excited states and integrated over the acceptance angle of spectrometer B. As seen in Fig. 6, the calculation reproduces the (deconvoluted) experimental energy loss spectrum well and shows that under the selected experimental conditions, a substantial part of intensity associated with the production of the $2p_{3/2,1/2}$ hole is pumped into $J\neq 1$ excited states.

B. Auger decay rates

The Auger transition rates were calculated by using the multiconfigurational Dirac-Fock representation of the $[2p_{3/2}]4s$

TABLE I. DDCS for the electron-impact excitation of jjJ-coupled $[np]n's$ and $[np]n'p$ states expressed in terms of the direct ($A_{m_i m_f}$) and the exchange ($B_{m_i m_f}$) amplitudes. The last column gives the relative EELS yields $N_\alpha^A/N_{\alpha_0}^A$ for spectrometer A, calculated according to Eq. (8). $|\alpha_0\rangle$ denotes the $[2p_{3/2}]4s$ ($J=1$) state.

l_i	j_i	l_f	j_f	J	$\sigma^J_{l_i j_i l_f j_f}$	$N_\alpha^A/N_{\alpha_0}^A$
1	1/2	s	1/2	0	$\frac{1}{36}\sum_{m=-1}^{1}\lvert B_{0m}\rvert^2$	0.22
1	1/2	s	1/2	1	$\frac{1}{36}\sum_{m=-1}^{1}(2\lvert A_{0m}\rvert^2+\lvert B_{0m}\rvert^2+2\lvert A_{0m}-B_{0m}\rvert^2)$	0.83
1	3/2	s	1/2	1	$\frac{1}{36}\sum_{m=-1}^{1}(\lvert B_{0m}\rvert^2+8\lvert A_{0m}-\frac{B_{0m}}{2}\rvert^2)$	1.00
1	3/2	s	1/2	2	$\frac{5}{36}\sum_{m=-1}^{1}\lvert B_{0m}\rvert^2$	1.12
1	3/2	p	3/2	0	$\frac{1}{108}(2\lvert 2A_{00}+4A_{11}-B_{00}-2B_{11}\rvert^2+\lvert B_{01}+B_{-10}\rvert^2)$	3.11
1	3/2	p	3/2	1	$\frac{1}{540}(4\lvert 2B_{00}+3B_{11}\rvert^2+2\lvert B_{00}+4B_{11}\rvert^2+\lvert B_{01}-B_{-10}\rvert^2+2\lvert 3B_{01}+2B_{-10}\rvert^2$ $+2\lvert 2B_{01}+3B_{10}\rvert^2+4\lvert B_{11}\rvert^2)$	0.26
1	3/2	p	3/2	2	$\frac{1}{108}(6\lvert 2A_{01}+B_{01}\rvert^2+2\lvert 2A_{00}-2A_{11}-B_{00}+B_{11}\rvert^2+6\lvert -2A_{01}+B_{-10}\rvert^2$ $+7\lvert B_{01}+B_{-10}\rvert^2+24\lvert A_{-11}-B_{10}/2\rvert^2)$	0.24
1	3/2	p	3/2	3	$\frac{7}{180}(2\lvert B_{00}-B_{11}\rvert^2+3\lvert B_{01}-B_{-10}\rvert^2+6\lvert B_{-11}\rvert^2)$	0.81
1	3/2	p	1/2	1	$\frac{1}{216}(4\lvert B_{00}+B_{11}\rvert^2+2\lvert B_{00}+3B_{11}\rvert^2+\lvert B_{-10}\rvert^2+2\lvert 2B_{01}+B_{-10}\rvert^2$ $+\lvert 2B_{01}+3B_{-10}\rvert^2+2\lvert B_{-11}\rvert^2)$	0.27
1	3/2	p	1/2	2	$\frac{1}{216}(6\lvert B_{00}-B_{11}\rvert^2+4\lvert 2A_{00}-2A_{11}-B_{00}+B_{11}\rvert^2+3\lvert 4A_{01}+2B_{01}-B_{-10}\rvert^2$ $+3\lvert -4A_{01}+B_{-10}\rvert^2+2\lvert B_{-10}-2B_{01}\rvert^2+24\lvert A_{-11}-B_{-11}\rvert^2$ $+24\lvert A_{-11}\rvert^2+12\lvert B_{-10}\rvert^2+6\lvert B_{-11}\rvert^2)$	0.57
1	1/2	p	3/2	1	$\frac{1}{216}(4\lvert B_{00}+B_{11}\rvert^2+2\lvert B_{00}+3B_{11}\rvert^2+\lvert B_{01}\rvert^2+2\lvert 2B_{-10}+B_{01}\rvert^2$ $+\lvert 2B_{-10}+3B_{01}\rvert^2+2\lvert B_{-11}\rvert^2)$	0.13
1	1/2	p	3/2	2	$\frac{1}{216}(6\lvert B_{00}-B_{11}\rvert^2+4\lvert 2A_{00}-2A_{11}-B_{00}+B_{11}\rvert^2+3\lvert 4A_{01}-2B_{-10}+B_{01}\rvert^2$ $+3\lvert 4A_{01}+B_{01}\rvert^2+2\lvert B_{01}-2B_{-10}\rvert^2+24\lvert A_{-11}-B_{-11}\rvert^2+24\lvert A_{-11}\rvert^2$ $+12\lvert B_{01}\rvert^2+6\lvert B_{-11}\rvert^2)$	0.21
1	1/2	p	1/2	0	$\frac{1}{108}(\lvert 2A_{00}+4A_{11}-B_{00}-2B_{11}\rvert^2+2\lvert B_{01}+B_{-10}\rvert^2)$	1.01
1	1/2	p	1/2	1	$\frac{1}{108}(2\lvert B_{00}\rvert^2+4\lvert B_{01}\rvert^2+\lvert B_{00}-2B_{11}\rvert^2+2\lvert B_{01}-B_{-10}\rvert^2+4\lvert B_{-10}\rvert^2+8\lvert B_{-11}\rvert^2)$	0.13

and $[2p_{3/2}]4p$ resonances and of the $[3p^2]nl$ final ionic states [33],

$$\sigma^A_{\alpha\beta} \propto \sum_j \left| \sum_{\alpha,\beta} c_\alpha c_\beta \langle \psi_\beta(J_\beta) E_b l j; J | \sum_{n>m} \frac{1}{r_{nm}} | \psi_\alpha(J) \rangle \right|^2, \tag{21}$$

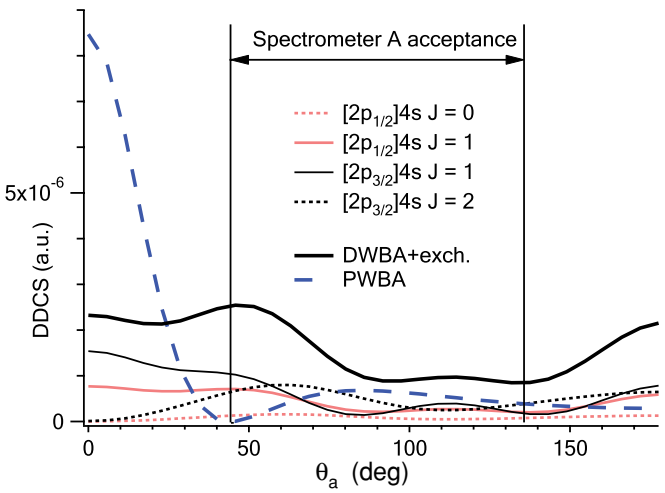

FIG. 5. (Color online) Calculated DDCS for excitation of Ar$[2p]4s$ states by the 350-eV electrons.

where ψ denotes a single configuration state function (CSF) and c_α and c_β are CSF weights of the resonant and final states, respectively. Our representation of argon $[2p_{3/2}]4s$ ($J=1,2$) resonances employs $[2p]4$–$5s,3$–$5d$ configurations, and the final states are represented by $[3p^2]4$–$6s,3$–$6d$ configurations. In this particular system, it was noted that besides the final state configuration interaction, the target relaxation upon Auger emission plays an important role in the decay. The relative participator contribution is usually estimated by the squared overlap integrals between fully relaxed radial orbitals of the intermediate and final states, respectively [5]. Here, we have calculated Auger matrix elements between fully optimized sets of radial orbitals, which automatically takes the shake-up process into account. The nonorthogonality was handled by the nonrelativistic code [34], and the Auger electron was described by the p wave of 210-eV energy, calculated in the field of the final ion state configuration.

The calculated Auger spectrum of $[2p_{3/2}]4s$ ($J=1$) resonance can be compared with the several published theoretical results for the total Auger yield (Ref. [12] and references therein), and with highly resolved resonant Auger spectra induced by the photon probe and recorded at the magic angle with respect to the polarization of the incoming light ([12,35]). Our experiment shows that relative intensities of the three dominant spectator features in an electron-impact spectrum (roughly denoted by ^3P:^1D:^1S) agree relatively well with the corresponding features in photoexcitation spectra

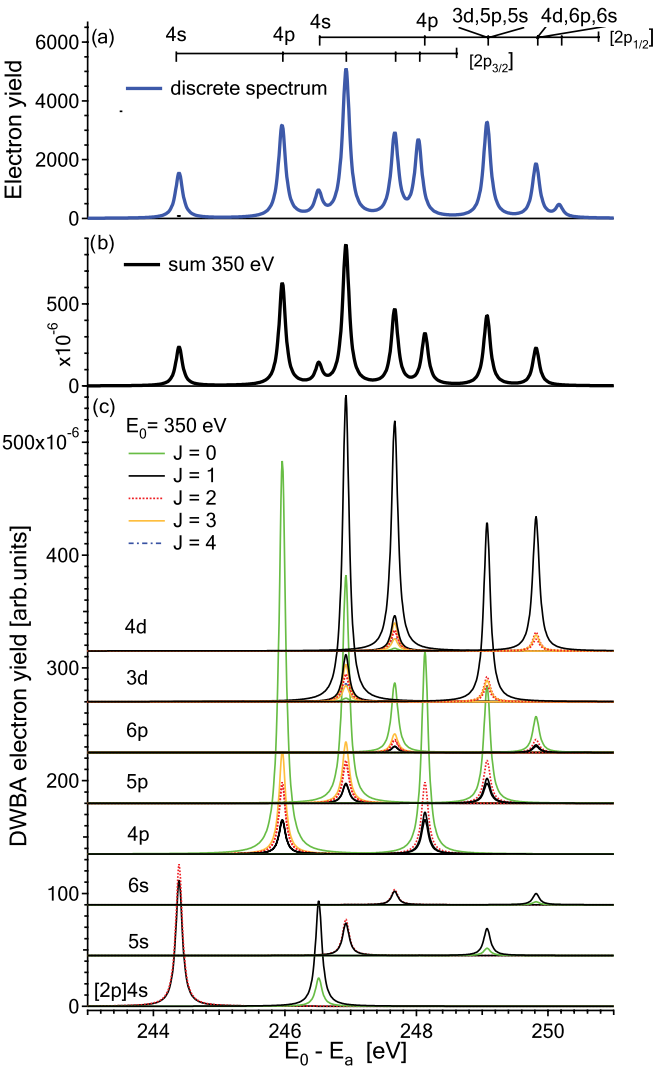

FIG. 6. (Color online) (a) The resonant part of the energy-loss spectrum in the region of Ar $2p$ edge extracted from the experimental data at $E_0 = 350$ eV [13]. (b) The calculated DWBA spectrum for the electron-impact energy of 350 eV (normalized to the experimental $[2p_{3/2}]4s$ peak intensity). (c) The decomposition of the DWBA spectrum into the different $[2p_{j_1}]nl_{j_2}(J)$ contributions.

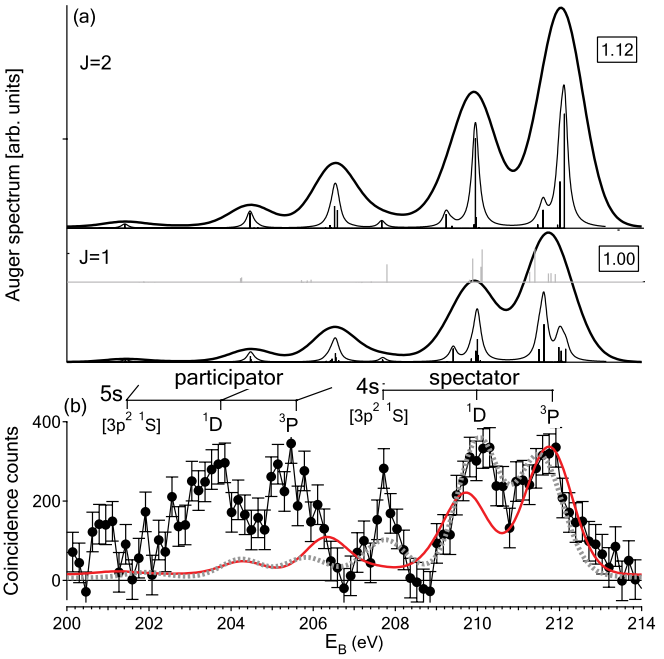

FIG. 7. (Color online) (a) The calculated L_3–$M_{23}M_{23}$ Auger spectrum of $[2p_{3/2}]4s(J)$ states for the total angular momentum $J = 1,2$. The spectra are broadened by the natural linewidth (thin line) and convoluted by experimental resolution (thick black line). (b) The experimental spectrum (black circles) compared to the sum of different J contributions, weighted by relative excitation strengths (denoted by a number in a box for each J) calculated for our experimental conditions (thick line). The strongest groups of final states are roughly denoted by $[LS]$ coupled $3p^2$ inner-valence holes and an orbital occupied by the outer electron. A highly resolved photoexcited resonant Auger spectrum from the measurement of Ref. [11] is also shown (dotted line). The corresponding spectral lines are presented by gray sticks in the $J = 1$ panel of (a).

approximately giving the ratio 1:1:0.25. This is in line with our calculations showing that similar spectral shapes are expected for $J = 1,2$ resonances when convoluted by the present instrumental resolution [Fig. 7(a)]. However, the $4s \rightarrow 5s$ shake-up probability in photoexcitation experiment is found to contribute only about 12% to an overall Auger intensity, which agrees well with the calculated shake-up probability, given by the $\langle 5s'|4s\rangle^2$ overlap factor [11]. From our measurements, it follows that the electron impact at 350 eV leads to the substantially increased shake-up probability with respect to the photoexcitation, with the participator decay being almost as probable as the spectator decay. This result obviously cannot be explained by an orbitals mixture required to present correlated spectator-participator final states, not even accounting for the (monopole) target relaxation.

There could be two reasons for such behavior. (i) The role of angular distribution of Auger electrons. It is well known from the photon probe experiments that resonant Auger electrons display anisotropic emission [36]. The asymmetry parameter β with respect to polarization of the incoming photon beam is different from zero for $4s$ ($J = 1$) resonance and assumes values ranging from -0.6 to 0.6 for different spectator transitions [12,35]. No similar data are available for the participator transitions. However, deGouw *et al.* [37] detected similar small shake-up components in photoexcitation, although their CMA spectrometer collected the signal over a large range of emission angles. (ii) The interference with the direct ionization process. According to this mechanism, the amplitude for direct production of the final state strongly interferes with the resonant process and effectively prevents separation of the two processes. When forced, the separation gives the apparently wrong spectator versus participator ratio. Let us try to estimate the possible effect of this error by inspection of Fig. 3(a). For our purpose, the resonant path (2) is split into the spectator R_S and participator R_P amplitudes, the same as the direct process (4), for which the spectator S_S and participator S_P amplitudes are defined by leading to the same final states in the corresponding energy interval. The difference of measured

signals, associated with the wrong participator-spectator ratio is then symbolically written as

$$\frac{|R_P \pm S_P|^2 - |S_P|^2}{|R_S \pm S_S|^2 - |S_S|^2} \approx 1, \tag{22}$$

where each part is expressed as a difference of on-the-resonance and off-the-resonance signals in Fig. 3(a). We take $S_S \approx 0$, which is supported by a relatively flat shape of the direct spectrum in the spectator region. The ratio of the two contributions in the absence of direct ionization process is then expressed as

$$\frac{|R_P|^2}{|R_S|^2} \approx \frac{1}{1 + 2(S_P/R_P)} \approx 0.16. \tag{23}$$

The interference has to be constructive to obtain an enhancement factor for the apparent participator spectral contribution with respect to the spectator part. The ratio in the denominator was obtained by assuming, again on the basis of Fig. 3(a), that $(R_P + S_P)^2/S_P^2 \approx 2$. The final results (23) for the true participator-to-spectator ratio almost reproduce the ratio from the photoexcitation spectrum, where the interference effects of such kinds are negligible [35]. Therefore, it could be possible that the participator-spectator probability ratio is increased for a factor of 5 in an electron-impact experiment because of the interference of the resonant with the direct ionization process.

Compared to the photoexcitation data [11], our $J = 1$ spectrum underestimates ^1S and ^1D spectator contributions. While the $^1D/^3P$ spectator ratio is too low in other calculations too (see Ref. [12]), this is due in part (10%) to omission of the f wave in the description of the Auger decay into ^1D final states. This is shown by a separate single configuration calculation with an orthogonal set of orbitals and both p and f waves for Auger electrons, which nearly reproduce the spectator part of the $[3p^2]4s$ ($J = 1$) spectrum [11]. The remaining disagreement is attributed to the averaging of radial orbitals over many configurations included in the description of the intermediate and final states. Although the intensities of different spectral features are not very well reproduced, the comparison with the experimental spectrum allows a rough assignment of the spectral features in terms of the LS coupled $3p^2$ holes and an electron orbital, occupied by an outer electron. The experimental resolution at present allows the observation of three groups of states for the spectator and for the participator channels, although the calculations reveal much more complex spectral structure due to the final state configuration interaction. For example, the final state with predominantly $[3p^2\,^3P]3d$ ($J = 1$) character contributes about 35% of intensity to the $[3p^2\,^1D]4s$ group of states.

Similarly, the Auger decay probabilities of $[2p_{3/2}]4p$ ($J = 0$–3) states were calculated employing $4p$–$5p$ orbitals for the configuration mixing. It is interesting that, while the convoluted spectra for $J = 0,2,3$ all resemble the measured spectral shape, the $J = 1$ spectrum strongly deviates from the experimental data in the spectator region (Fig. 8). This indicates that the $J = 1$ resonant path is probably of minor importance, as expected on the basis of calculated relative excitation probabilities $N_\alpha^A/N_{\alpha_0}^A$, given in the Appendix (Table I). Less obvious as in the case of $[2p_{3/2}]4s$, but still clearly notable, the shake-up contribution is underestimated by the present model for about a factor of 2. The experimental result therefore suggests that about 30% of the Auger decay is of the participator type, while the shake-up overlap $\langle 5p'|4p\rangle^2 \approx 0.15$. Again, a part of the missing intensity of the ^1D spectator group of lines, but not more than 10% of the p-wave intensity, could be attributed to the omission of the f wave in the Auger electron representation.

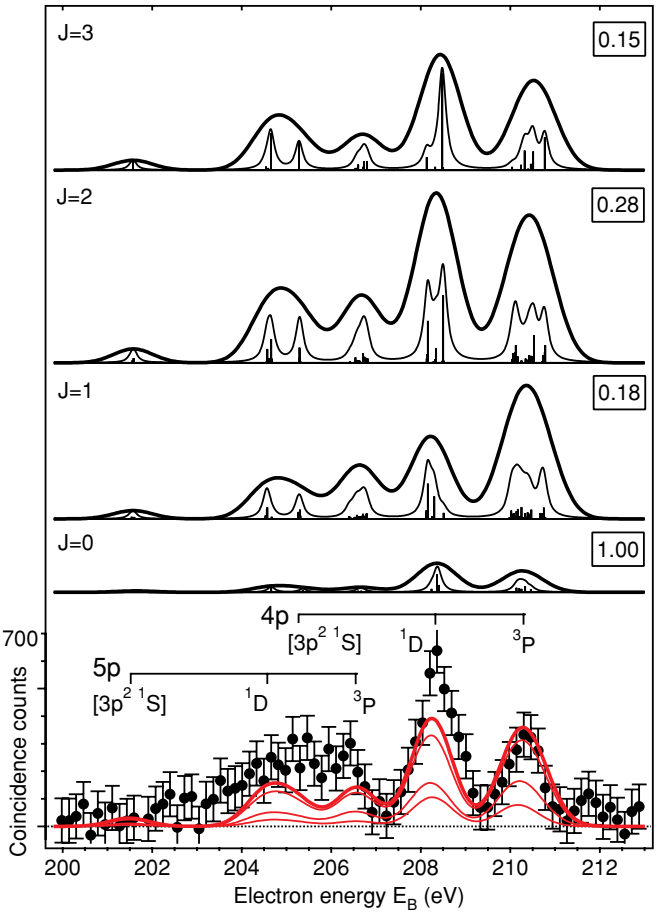

FIG. 8. (Color online) The $[2p_{3/2}]4p(J) \rightarrow [3p^2]4$–$5p, Ep$ Auger spectra, calculated for the different values of the total angular momenta J. The spectra are broadened by the natural linewidth (thin line) and convoluted by the experimental resolution (thick black line). The calculated relative excitation strengths are given in a box for each J. Bottom, the experimental spectrum is compared to the sum of the different J contributions, weighted by the relative excitation strengths at 350-eV electron-impact energy (thick red line). A sequence of thin (red) lines shows the evolution of the calculated spectrum upon addition of progressively higher J components.

IV. CONCLUSIONS

The resonant Auger spectra of $[2p_{3/2}]4s(J)$ and $[2p_{3/2}]4p(J)$ group of states in argon have been measured by the $(e,2e)$ technique upon excitation by 343.6- and 344.9-eV electrons, respectively. These results represent the experimental evidence of the resonant Auger decay involving a well-resolved group of inner-shell excited atomic states

produced by an electron impact. In particular, the resonant Auger spectrum of $[2p_{3/2}]4p$ states, inaccessible by photoexcitation, is reported. The identification of a weak signal, previously found by the noncoincidence experiment is confirmed by the present coincidence measurements. The observed spectator structure of $\mathrm{Ar}[2p_{3/2}]4s(J)$ Auger spectrum matches the properly convoluted photoexcitation data in shape, although the calculations indicate about equal contribution of $J = 1,2$ excited states in the electron-impact experiment. According to the DWBA scattering model and the calculated Auger rates, the largest contributions to the $[2p_{3/2}]4p$ spectrum in our experimental geometry originate from $J = 0,2$ excited states. It was found that the probability of the shake-up process is significant, especially for the $4s$ relaxation where the 10% ratio from the photon probe experiments is surpassed by a factor of 5. The interference of the resonant Auger path with the direct outer-shell ionization may be responsible for such an effect, but the corresponding calculations are needed. Better energy-resolved measurements in the future are expected to reveal much more spectroscopic details about the electron-induced resonant Auger decay.

ACKNOWLEDGMENTS

This work is supported by the research programme P1-0112 of the Slovenian Research Agency and by the TT Grant No. SLO-15/05 (BI/HU-06-07-015).

APPENDIX

DWBA cross sections $\sigma^J_{l_i j_i l_f j_f}$ as given by Eq. (17) in terms of the direct Eq. (18) and the exchange Eq. (19) amplitudes are reported in Table I for jjJ-coupled $[np]ns,np$ configurations. In our case, to represent the physical states, both $[2p_{3/2}]4p$ $(J = 1)$ states have to be mixed into $3/2[K = 1/2,3/2]$ $(J = 1)$ states (and similarly for the $2p_{1/2}$ hole). For the $[np]ns$ configuration, it can easily be shown that $A_{0-m} = -A_{0m}$ and $B_{0-m} = B_{0m}$ when $m \neq 0$ and that summation over all possible j_i, j_f, J angular momenta leads to the familiar expression for electron-electron scattering cross sections [38],

$$\sum_{j_i,j_f,J} \sigma^J_{l_i j_i l_f j_f} = \sum_{m=-1}^{1} (|A_{0m}|^2 + |B_{0m}|^2 + |A_{0m} - B_{0m}|^2). \tag{A1}$$

[1] H. Aksela, S. Aksela, H. Pulkkinen, G. M. Bancroft, and K. H. Tan, Phys. Rev. A **37**, 1798 (1988).
[2] L. O. Werme, T. Bergmark, and K. Siegbahn, Phys. Scr. **8**, 149 (1973).
[3] P. Eisenberger, P. M. Platyman, and H. N. Winick, Phys. Rev. Lett. **36**, 623 (1976).
[4] A. Kivimäki, A. Naves de Brito, S. Aksela, O.-P. Sairanen, A. Ausmees, S. J. Osborne, L. B. Dantas, and S. Svensson, Phys. Rev. Lett. **71**, 4307 (1993).
[5] M. Meyer, E. v. Raven, B. Sonntag, and J. E. Hansen, Phys. Rev. A **43**, 177 (1991).
[6] R. Camilloni, M. Žitnik, C. Comicioli, K. C. Prince, M. Zacchigna, C. Crotti, O. Ottaviani, C. Quaresima, P. Perfetti, and G. Stefani, Phys. Rev. Lett. **77**, 2646 (1996).
[7] G. C. King, M. Tronc, F. H. Read, and R. C. Bradford, J. Phys. B **10**, 2479 (1977).
[8] H. Aksela and J. Mursu, Phys. Rev. A **54**, 2882 (1996).
[9] B. Paripás, G. Vikor, and S. Ricz, J. Phys. B **30**, 403 (1997).
[10] A. Hiltunen *et al.*, J. Electron Spectrosc. Relat. Phenom. **87**, 203 (1998).
[11] J. Mursu *et al.*, J. Phys. B **29**, 4387 (1996).
[12] A. Farhat, M. Humphrey, B. Langer, N. Berrah, J. D. Bozek, and D. Cubaynes, Phys. Rev. A **56**, 501 (1997).
[13] M. Žitnik *et al.*, Nucl. Instrum. Methods B **267**, 260 (2009).
[14] M. J. Brunger, O. Samardzic, A. S. Kheifets, and E. Weigold, J. Phys. B **30**, 3267 (1997).
[15] N. L. S. Martin, D. B. Thompson, R. P. Bauman, and M. Wilson, Phys. Rev. Lett. **72**, 2163 (1994).
[16] V. Feyer *et al.*, J. Phys. B **40**, F35 (2007).
[17] V. Feyer, P. Bolognesi, M. Coreno, K. C. Prince, and L. Avaldi, J. Electron Spectrosc. Relat. Phenom. **161**, 17 (2007).
[18] L. Avaldi, P. Bolognesi, R. Camilloni, E. Fainelli, R. A. Multari, and G. Stefani, Phys. Rev. A **54**, 2930 (1996).
[19] B. Paripás and B. Palásthy, Radiat. Phys. Chem. **76**, 565 (2007).
[20] B. Paripás and B. Palásthy, Nucl. Instrum. Methods B **267**, 275 (2009).
[21] A. Kikas *et al.*, J. Electron Spectrosc. Relat. Phenom. **77**, 241 (1996).
[22] S. Cvejanović, G. W. Bagley, and T. J. Reddish, J. Phys. B **27**, 5661 (1994).
[23] D. A. Shaw, G. C. King, F. H. Read, and D. Cvejanović, J. Phys. B **15**, 1785 (1982).
[24] C. E. Bielschowsky, G. G. B. de Souza, C. A. Lucas, and H. M. Boechat Roberty, Phys. Rev. A **38**, 3405 (1988).
[25] X. W. Fan and K. T. Leung, Phys. Rev. A **62**, 062703 (2000).
[26] M. P. de Miranda and C. Bielschowsky, J. Mol. Struct. **282**, 71 (1993).
[27] J. W. Cooper, Phys. Rev. **128**, 681 (1962).
[28] M. Kavčič and Ž. Šmit, Phys. Rev. A **79**, 052708 (2009).
[29] M. Kato *et al.*, J. Electron Spectrosc. Relat. Phenom. **160**, 39 (2007).
[30] M. Inokuti, Rev. Mod. Phys. **43**, 297 (1971).
[31] C. Schröter, L. Avaladi, R. Camilloni, G. Stefani, M. Žitnik, and M. Štuhec, J. Phys. B **32**, 171 (1999).
[32] D. H. Madison, R. V. Calhoun, and W. N. Shelton, Phys. Rev. A **16**, 552 (1977).
[33] K. G. Dyall, I. P. Grant, C. T. Johnson, F. A. Parpia, and E. P. Plummer, Comput. Phys. Commun. **55**, 425 (1989).
[34] O. Zatsarinny, Comput. Phys. Commun. **98**, 235 (1996).
[35] H. Aksela, J. Mursu, J. Jauhiainen, E. Nommiste, J. Karvonen, and S. Aksela, Phys. Rev. A **55**, 3532 (1997).
[36] T. A. Carlson, D. R. Mullins, C. E. Beall, B. W. Yates, J. W. Taylor, D. W. Lindle, and F. A. Grimm, Phys. Rev. A **39**, 1170 (1989).
[37] J. A. deGouw, J. van Eck, A. C. Peters, J. van der Weg, and H. G. M. Heideman, J. Phys. B **28**, 2127 (1995).
[38] C. J. Joachain, *Quantum Collision Theory* (North-Holland Publishing Company, North-Holland, 1975).